**Journal of Pathology**
*J Pathol* 2015
Published online in Wiley Online Library
(wileyonlinelibrary.com) DOI: 10.1002/path.4506

**ORIGINAL PAPER**

# Identification of novel vascular projections with cellular trafficking abilities on the microvasculature of pancreatic ductal adenocarcinoma

Hexige Saiyin,[1†*] Christine M Ardito-Abraham,[2†] Yanhua Wu,[1] Youheng Wei,[1] Yuan Fang,[2] Xu Han,[2] Jianang Li,[2] Ping Zhou,[1] Qing Yi,[3] Anirban Maitra,[4,5] Jun O Liu,[6] David A Tuveson,[2] Wenhui Lou[2*] and Long Yu[1*]

[1] *State Key Laboratory of Genetic Engineering, School of Life Sciences, Fudan University, Shanghai, People's Republic of China*
[2] *Cold Spring Harbor Laboratory, Cold Spring Harbor, NY, USA*
[3] *General Surgery Department, Zhongshan Hospital, Fudan University, Shanghai, People's Republic of China*
[4] *Cleveland Clinic, Lerner Research Institute, Cleveland, OH, USA*
[5] *Department of Pathology, University of Texas MD Anderson Cancer Center, Houston, TX, USA*
[6] *Departments of Pharmacology and Oncology, Johns Hopkins School of Medicine, Baltimore, MD, USA*

**Correspondence to: S Hexige and W Lou, State Key Laboratory of Genetic Engineering, School of Life Sciences, Fudan University, Shanghai 200433, People's Republic of China. E-mail: saiyin@fudan.edu.cn and longyu@fudan.edu.cn*
*Or L Yu, General Surgery Department, Zhongshan Hospital, Fudan University, Shanghai, People's Republic of China. E-mail: wenhuilou@aliyun.com*

[†]These authors contributed equally to this study.

## Abstract

**Pancreatic ductal adenocarcinoma (PDAC) is a nearly lethal neoplasm. It is a remarkably stroma-rich, vascular-poor and hypo-perfused tumour, which prevents efficient drug delivery. Paradoxically, the neoplastic cells have robust glucose uptake, suggesting that the microvasculature has adopted an alternative method for nutrient uptake and cellular trafficking. Using adapted thick tumour section immunostaining and three-dimensional (3D) construction imaging in human tissue samples, we identified an undiscovered feature of the mature microvasculature in advanced PDAC tumours; long, hair-like projections on the basal surface of microvessels that we refer to as 'basal microvilli'. Functionally, these basal microvilli have an actin-rich cytoskeleton and endocytic and exocytic properties, and contain glucose transporter-1 (GLUT-1)-positive vesicles. Clinically, as demonstrated by PET–CT, the tumour microvasculature with the longest and most abundant basal microvilli correlated with high glucose uptake of the PDAC tumour itself. In addition, these basal microvilli were found in regions of the tumour with low GLUT-1 expression, suggesting that their presence could be dependent upon the glucose concentration in the tumour milieu. Similar microvasculature features were also observed in a K-Ras-driven model of murine PDAC. Altogether, these basal microvilli mark a novel pathological feature of PDAC microvasculature. Because basal microvilli are pathological features with endo- and exocytic properties, they may provide a non-conventional method for cellular trafficking in PDAC tumours.**
Copyright © 2015 Pathological Society of Great Britain and Ireland. Published by John Wiley & Sons, Ltd.

**Keywords:** 3D imaging; pancreas; neoplasia; microvessels; basal microvilli

Received 15 July 2014; Revised 8 December 2014; Accepted 30 December 2014

*No conflicts of interest were declared.*

## Introduction

Pancreatic ductal adenocarcinoma (PDAC) is a near-uniformly lethal tumour [1]. The extremely poor prognosis for PDAC patients is partially due to resistance to conventional therapeutic modalities [2,3]. Despite intensive efforts, there are no truly effective therapies available for treating PDAC patients at the moment [4]. One proposed mode of resistance is that elevated interstitial pressures and hypovascularity of PDAC leads to hypoperfusion and decreased delivery of chemotherapy to the PDAC milieu [5,6]. Interestingly, PDAC tumours still manage to have a high glucose uptake, as assessed by fluoro-deoxyglucose positron emission tomography ($^{18}$FDG–PET) scans [7]. Clinical data have shown that the high glucose uptake:perfusion ratio correlates with a poor outcome for PDAC patients, suggesting that PDAC tumours do not have to be highly perfused to be highly metabolically active [8].

MRI and CT angiography, the standard imaging methods for visualizing vessel perfusion, only visualize blood vessels >100 µm in diameter [9]; however, microvessels involved in nutrient or drug exchange are far smaller [10]. Additionally, pathologists are limited by the use of thin biopsy sections, which lack the tissue depth needed to fully observe the multi-dimensional nature of the tumour microvasculature [11]. Altogether, this means that it is impossible to visualize the entire

Copyright © 2015 Pathological Society of Great Britain and Ireland.
Published by John Wiley & Sons, Ltd. www.pathsoc.org.uk

microvasculature by standard imaging methods. Due to these technical limitations, we hypothesized that the PDAC microvasculature may contain undetected and under-appreciated ultrastructural characteristics. Our aim was to design a better imaging method that would be capable of revealing novel characteristics of microvessels. We immunostained thick (45 μm) tumour tissue sections from human PDAC samples and used imaging reconstruction to visualize the tumour microvasculature in three dimensions (3D), allowing us to analyse its fine architecture. We reveal a novel type of microvessel that contains long, hair-like projections on the basal surface. We named these vascular microstructures 'basal microvilli', based on their location and the morphological resemblance to microvillus projections. Basal microvilli have cellular trafficking properties, contain GLUT1-positive vesicles and are prevalent in human PDAC tumours with high glucose uptake, suggesting their possible role in facilitating cellular uptake and trafficking between tumour cells and the microenvironment. As PDAC tumours are hypoperfused, these basal microvilli may provide a non-conventional bypass mechanism for nutrient uptake in PDAC microvessels.

## Materials and methods

Detailed information is provided in Supplementary materials and methods and Figures SM1 and SM2 (see supplementary material).

### Patients and immunohistochemistry

The research was approved by the Clinical Ethical Committee of Zhongshan Hospital, Fudan University. This study included 120 cases of PDAC, 59 cases of HCC and four cases of PanNET. All patients had surgical tumour resection at General Surgery Unit or Liver Surgery Unit of Zhongshan Hospital at Fudan University between January 2005 and September 2013. Six samples of haemangioblastomas (HBs) were kindly provided by Dr Liangfu Zhou and Ying Wang of Huashan hospital (China). For immunostaining, heat-mediated antigen retrieval was performed with sodium citrate buffer, pH 6.0, incubation with primary antibodies at 4 °C overnight and detection with peroxidase streptavidin–biotinylated complex and DAB/$H_2O_2$. For 3D image reconstruction, fresh tumour samples were fixed in freshly prepared 4% PFA overnight and cryoprotected in 30% sucrose/PBS. Thick (45 μm) tissue sections were immunostained [12] and scanned using a Zeiss 710 confocal microscope; 3D image reconstruction was performed in Zen 2012 imaging software (Zeiss, Germany).

### Microvessel parameters and measurements of basal microvilli

Slides were examined at low magnification and the most vascularized region was selected under ×20 magnification. Three to 10 optical fields were analysed in the tumour region of each slide and, if the sample included non-neoplastic pancreatic tissue, another three to 10 fields were also captured. Areas with a dense leukocytic or haemorrhagic infiltration and necrosis were excluded, as were vessels with muscular walls. We used ImageJ software to calibrate microvessel parameters [13]. Z-stacks of the entire microvasculature, including the basal microvilli, were scanned and then analysed by maximum intensity in ImageJ. We measured the total surface area of microvessels, quantified the basal microvilli on each microvessel and measured their lengths.

### Statistical analysis

Differences between categorical variables were assessed using one-way ANOVA or Pearson's or Spearman's correlations (two-tailed): continuous variables were compared using the bivariate correlation. Survival curves were estimated by the Kaplan–Meier method and differences assessed by log-rank test. The clinical pathological variables included in this analysis were: gender; age; tumour location (pancreas head, pancreas body–tail and entire pancreas); tumour stage (T1 + T2 versus T3 + T4); differentiation (G1, G2 and G3); regional lymph status (Yes versus No); metastasis (Yes versus No); TNM (I + II versus III + IV); vascular invasion (Yes versus No); and perineuronal invasion (Yes versus No). Microvessel parameters included microvessel density (MVD), microvessel coverage (%), perimeter and size.

## Results

### Human PDAC contains a mature, angiostatic, vascular network

To comprehensively characterize the microvessel characteristics in PDAC patients, we immunostained microvessels of thin (5 μm) paraffin sections from PDAC patient samples with the endothelial marker CD34 to image the tumour microvasculature. Then, according to pathological standards, we measured several microvessel parameters: microvessel density (MVD), ie the number of microvessels in a given area; size (area of the microvessel); percentage coverage, ie percentage of microvessels in a given area/total area; and perimeter, ie the distance around the microvessel. We measured the microvessel parameters in PDAC ($n = 86$), a hypovascularized cancer, in hepatocellular carcinoma (HCC, $n = 39$), a neoangiogenic cancer [14] and in the normal pancreas ($n = 57$). The average MVD in PDAC was 26.5% that of the normal pancreas and 50.0% that of HCC (Figure 1A). The microvessel coverage in PDAC was 40.0% of the normal pancreas and 28.6% of HCC (see supplementary material, Figure S1A). The average size of microvessels in PDAC was 56.7% of HCC and almost twice that of the normal pancreas (Figure 1A). The average perimeter of microvessels in PDAC was

Copyright © 2015 Pathological Society of Great Britain and Ireland.
Published by John Wiley & Sons, Ltd. www.pathsoc.org.uk

slightly longer ($55.2 \pm 14.22$ μm) than that observed in the pancreas ($41.2 \pm 7.75$ μm) and shorter than observed in HCC ($69.1 \pm 16.94$ μm; see supplementary material, Figure S1A). PDAC tumour vessels appeared to lack a branching phenotype, as is commonly seen in angiogenic tumours such as those observed in HCC (see supplementary material, Figure S1B). Higher magnification revealed that the morphology of the microvessels in PDAC resembled the structure of normal pancreatic microvessels, but differed from the large, dilated microvessels of HCC (Figure 1B). It is noteworthy that no other significant correlations were observed between the microvessel parameters and the prognoses of patients or clinical pathology, including age, gender, location of tumour, tumour stage, regional lymph node status, metastases, TNM and tumour differentiation (see supplementary material, Figure S1C, Table S1), consistent with a previous report [15].

Angiogenesis in solid tumours is initiated by vascular endothelial growth factor (VEGF), which is released by tumour cells in a hypoxic environment in response to hypoxia-inducible factor (HIF-1α) [16]. Typically, VEGF induced-neoangiogenic microvessels in solid tumours have a dilated lumen [17]; however, PDAC tumours microvessels have been reported to be compressed and hypoperfused [18,19]. To determine whether human PDAC tumours have hypoxia-induced, VEGF-mediated angiogenesis, we used tissue microarrays to compare the expression patterns of HIF-1α and VEGFR2 by immunohistochemistry. To avoid problems of tumour heterogeneity, three to six images of each tissue were taken to reduce the bias in each sample. HIF-1α expression was strong in only one of 12 PDAC samples by immunoblotting (see supplementary material, Figure S2A). Immunohistochemistry revealed varying degrees of HIF-1α expression in 88/197 patients (see supplementary material, Figure S2B). Additionally, HIF-1α was expressed in neoplastic cells, but mostly in endothelial cells and precancerous lesions in PDAC tumours (see supplementary material, 2B). Contrary to a previous report [20], we failed to find any correlation between microvessel parameters, including percentage microvessel coverage and microvessel size, and HIF-1α expression level in PDAC patients (see supplementary material, Figure S2B). Consistent with a previous report [21], we detected HIF-1α expression in all HCC (13/13) and liver (3/3) samples (see supplementary material, Figure S2D). HIF-1α expression level in HCC patients correlated positively with increased percentage of microvessel coverage and size. HCC tumours with higher levels of HIF-1α had a higher percentage of microvessel coverage and more dilated microvessels (see supplementary material, Figure S2D, E). In PDAC tumour samples, VEGFR2 was expressed in precancerous lesions and in a limited number of tumour cells, but not in endothelial cells (see supplementary material, Figure S2C), whereas VEGFR2 was widely expressed in tumour cells, endothelial cells and infiltrating inflammatory cells in most of the HCC tumours (see supplementary material, Figure S2F). Although hypoxia is severe in PDAC [22], spatial and heterogeneous expression patterns of HIF-1α and VEGFR2 imply that the paradigm for hypoxia-induced angiogenesis may not apply universally to PDAC tumours.

Neoangiogenic vessels form from terminal endothelial cells and/or branch points of pre-existing vessels, which is accomplished by tip-stalk cell fate specification mediated by VEGF–Notch signalling [23]. A newly-formed, immature sprout is commonly identified by proliferating stalk cells next to the terminal end UNC5B-positive tip cell with filapodia [24]. These new sprouts are marked by the presence of nascent pericytes, or even the absence of pericytes and basal membrane [24]. Because of the significantly lower MVD and size of PDAC microvessels, we hypothesized that the human PDAC microvasculature is non-angiogenic, or angiostatic. To assess this possibility, we systematically analysed immunostained PDAC and HCC tumour sections for the presence of tip cells, proliferating endothelial cells, pericyte coverage and basement membrane integrity. In HCC tumour tissues, we observed two types of endothelial tip cells with filopodia, one at the branch points of pre-existing microvessels and the other at the tips of microvessels (see supplementary material, Figure S1D). In contrast, there were no terminal endothelial cells with filopodia in the PDAC microvessels (Figure S1D). To assess angiogenesis in the tumour microvasculature, we co-immunostained tissues with the endothelial marker CD34, the proliferation marker Ki67 and the endothelial tip cell marker UNC5B. Normally, UNC5B is expressed in the developing vasculature [25] and in tumours where angiogenesis is robust. We observed proliferating endothelial cells at the terminal ends or branch points of HCC microvessels (Figure 1C). However, in PDAC tumours, no proliferating endothelial cells were observed at the terminal ends of the microvessels (Figure 1C). Only a small number of proliferating cells could be observed in the microvessel wall, which is considered to be the result of normal turnover activity [26]. Quantitatively, the ratio of proliferating endothelial cells to microvessels in HCC was significantly higher than that in PDAC (Figure 1C) and there was a significantly higher UNC5B-positive endothelial cell:microvessel ratio in HCC compared to PDAC, where there were no detectable UNC5B-positive endothelial cells (Figure 1D). Given the small number of $Ki67^+$ cells we observed in the PDAC microvasculature (of the four samples, we observed only three $Ki67^+$ endothelial cells) and their location (not at the terminal end of a pre-existing microvessel), these proliferative endothelial cells in PDAC are presumably due to normal turnover and not angiogenesis.

Next, we evaluated the pericyte coverage of microvessels in PDAC compared to HCC tissue samples by co-immunostaining with markers for nascent and mature pericytes [NG2 and platelet-derived growth factor receptor (PDGFR)-β, nascent; desmin and smooth muscle actin (SMA), mature] in combination with endothelial markers (CD31 or CD34). We found that 16.7% of microvessels in HCC were devoid of mature,

Copyright © 2015 Pathological Society of Great Britain and Ireland.
Published by John Wiley & Sons, Ltd. www.pathsoc.org.uk

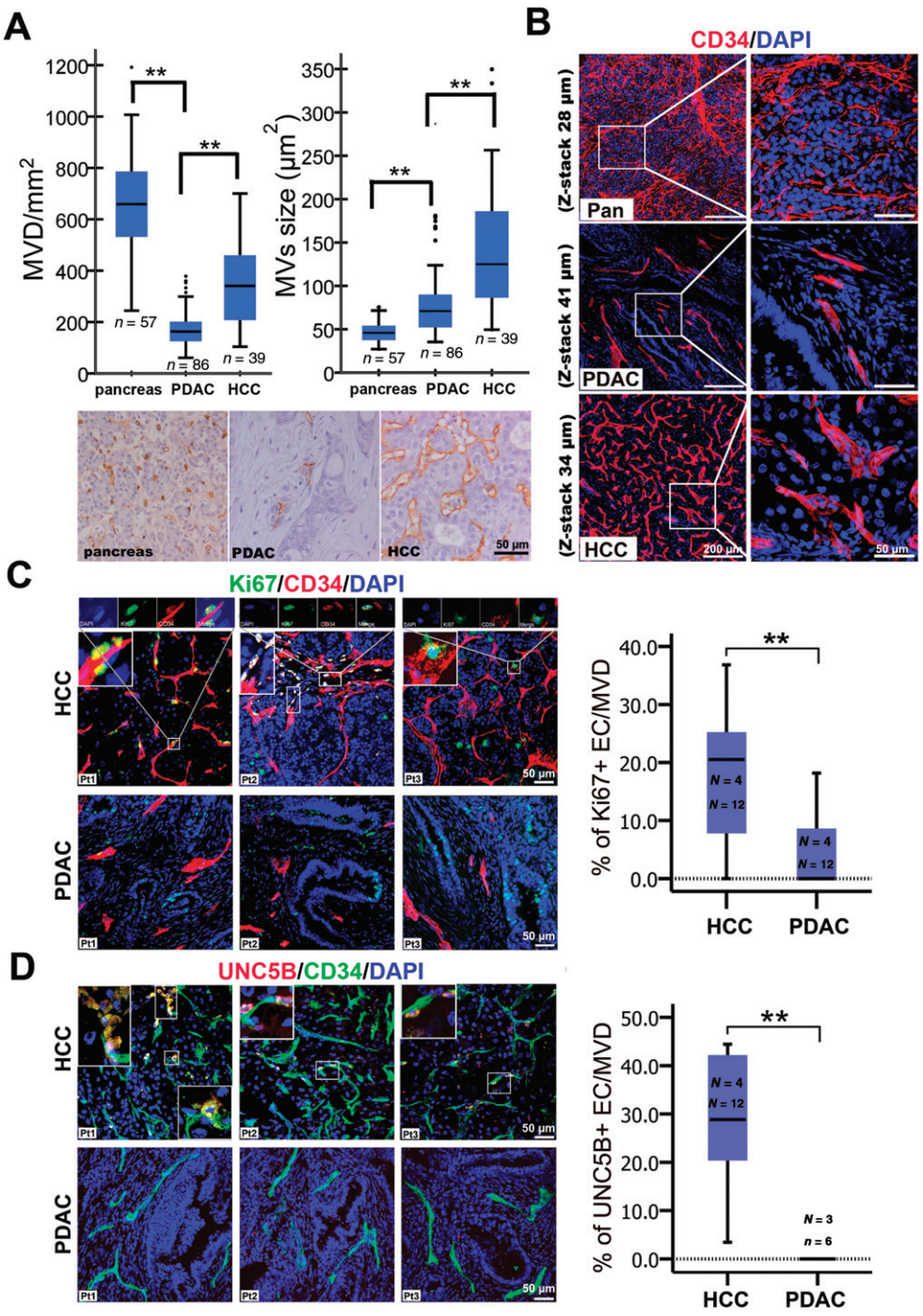


**Figure 1.** Human PDAC contains an angiostatic vascular network. (A) Comparison of standard microvessel parameters of PDAC with those of pancreas and of HCC; $^{**}p < 0.01$, using one-way ANOVA. (B) 3D images of CD34 immunostained microvessel network in human PDAC, pancreas and HCC tissues. (C) Comparison of proliferating endothelial cells in PDAC with that in HCC; boxed panels show Ki67-positive endothelial cells in HCC located at the tip of a microvessel [Patient (Pt)1)], having migrated from the tips of microvessels (Pt2) or at the branch points of microvessels (Pt3). (D) Comparison of UNC5B-positive endothelial cells in PDAC with those in HCC; boxed panels show UNC5B-positive endothelial cells migrating from the top of microvessels (Pt1, upper left) and UNC5B-positive endothelial cells at the branch points of microvessels (Pt1 and Pt2, lower right) or located at the tip of microvessels in HCC (Pt2 and Pt3). Total UNC5B-positive endothelial cells/microvessels counts in HCC (138/500) and PDAC (0/77), UNC5B-positive cells/total microvessels count; EC, endothelial cells. Statistical significance was assessed by Student's *t*-test; N, number of patients; n, number of images examined; values are mean ± SD.

SMA-positive pericyte coverage, but that all microvessels in PDAC were covered by SMA-positive pericytes (see supplementary material, Figure S3A, Table S2). In contrast to the intense staining in stromal cells, most of the microvessel pericytes in PDAC showed weak desmin and PDGFRβ expression (see supplementary material, Figure S3B, C). A small number of nascent NG2-positive microvessel pericytes were observed in PDAC, and those pericytes covered the ends of smaller microvessels (see supplementary material, Figure S3D). In contrast, we counted a significant number of NG2- and PDGFRβ-positive nascent pericytes in HCC

Copyright © 2015 Pathological Society of Great Britain and Ireland.
Published by John Wiley & Sons, Ltd. www.pathsoc.org.uk

microvessels (see supplementary material, Table S2). These nascent pericytes were located at the ends of microvessels or were attached to the branching points of microvessels (see supplementary material, Figure S3C, D). Desmin-positive pericytes in HCC appeared to be loosely attached to the main branches of microvessels (Figure S3B).

Analysis of the PDAC microvasculature demonstrated a non-proliferative, angiostatic state. Therefore, we hypothesized that PDAC microvessels were of a more mature, co-opted nature than the highly angiogenic vasculature seen in HCC. To test this, we evaluated the integrity of the microvessel basement membrane as a measurement for vessel maturity in PDAC and HCC by using triple immunofluorescent staining for mature pericytes, endothelial cells and basement membrane type IV collagen. The microvessels in PDAC had a complete basement membrane that was covered with pericyte processes (see supplementary material, Figure S4A). However, the microvessels in HCC had an incomplete basement membrane, with some regions of the basal surface not covered by type collagen IV on the basement membrane at all (Figure S4A). We examined the endothelial junctions by transmission electron microscopy (TEM) and found that microvessels in PDAC were connected to each other by junctional complexes including tight junctions and intermediate junctions (see supplementary material, Figure S4B). Altogether, these results indicate that HCC tumour vessels are immature and angiogenic, while the PDAC vascular network is mature and angiostatic.

## Novel 'basal microvilli' are vascular projections with an actin cytoskeleton and endo- and exocytic properties on the basal surfaces of PDAC microvessels

These data indicated that PDAC tumours have a low MVD and a lack of angiogenesis, so we questioned how the tumour cells obtain their nutrients and clear cellular waste to support their growth in the absence of an extensive vascular network. While characterizing the PDAC vasculature in tissue samples, we discovered many hair-like, fine vascular projections from the basal surface of most microvessels in human PDAC tumours. These endothelial-derived, basal projections were widely distributed across the microvessels, measuring about 0.8–1.2 μm in diameter (Figure 2A; see also supplementary material, Movie S1). In contrast, the basal surfaces of the microvessels in normal human pancreata ($n = 3$) and HCC ($n = 6$) lacked these vascular projections (Figure 2A; see also supplementary material, Movie S1). The lengths of the basal projections were in the range 3–41 μm and there were about $0.2 \times 10^5 - 1.3 \times 10^5$ microprojections/mm$^2$ of a PDAC microvessel. Strikingly, some of the longest projections transversed the perivascular stroma and invaded the neoplastic epithelium (Figure 2B). These endothelial projections do not express another prominent endothelial marker, CD31 (Figure 2C). Additionally, we immunostained for GLUT-1, a glucose transporter highly expressed in red blood cells (RBCs) [27], to determine whether the microvascular projections were connected to microvessels with an active blood flow and, in fact, we detected GLUT-1-positive RBCs in the microvessels connected to the endothelial microprojections (see supplementary material, Figure S5A).

The functional nature of apical projections in polarized epithelial cells depends on their cytoskeletal properties. Cytoskeletal tubulin is necessary for dynamic movement and the actin cytoskeleton is necessary for absorptive or secretive functions [28,29]. We co-immunostained tissues with the cytoskeletal markers phalloidin (F-actin) or α-tubulin and CD34 to further characterize the basal microvilli. Co-immunostaining demonstrated that the cytoskeleton of these projections do not contain tubulin, but contain actin microfilaments that connect to actin filaments of the endothelial cells, similar to how stereocilia and microvilli attach to the cytoplasm of a cell (Figure 2D, E; see also supplementary material, Figure S5B).

Endocytosis is the main method by which cells take up and transport macromolecules and this process can be either clathrin-dependent or clathrin-independent [30]. To determine whether basal microvilli have endocytic capacity, we co-immunostained for CD34 and clathrin or β-COP, a marker for clathrin-independent vesicles, and discovered that basal microvilli contain both types of vesicles (Figure 3A, B). Transmission electron microscopy (TEM) revealed that these fine microvascular projections contain pinocytic vesicles, phagocytic bodies, macropinocytic pseudopodia and large exocytic vesicles, as well as rough endoplasmic reticulum and mitochondria (Figure 3C). Altogether, these data suggested that these microvascular projections in PDAC tumours may function to increase nutrient transport and waste clearance.

Based on these data, we named these endothelial-derived basal projections 'basal microvilli' because of their actin-rich cytoskeleton. Basal microvilli were only observed in malignant, aggressive and metastatic PDAC tumours, but not in non-invasive precursor lesions, including pancreatic intraepithelial neoplasia (PanIN)-1, PanIN-2 and PanIN-3 (see supplementary material, Figure S5C–F). Also, we observed basal microvilli on microvessels in normal pancreas tissue in proximity to the neoplastic regions of GLUT-1-positive tumours (see supplementary material, Figure S5E, F, Movie S2). These data suggested that basal microvilli are not a physiological, but a pathological, phenomenon that arises only in the setting of invasive PDAC.

## Basal microvilli have low levels of phosphorylated VEGFR2

Angiogenesis is induced by tumour production and release of VEGF, the ligand responsible for activating the receptor tyrosine kinase VEGFR2 under hypoxic conditions [16]. VEGF-bound VEGFR2 induces autophosphorylation of specific tyrosine residues

Copyright © 2015 Pathological Society of Great Britain and Ireland.
Published by John Wiley & Sons, Ltd. www.pathsoc.org.uk

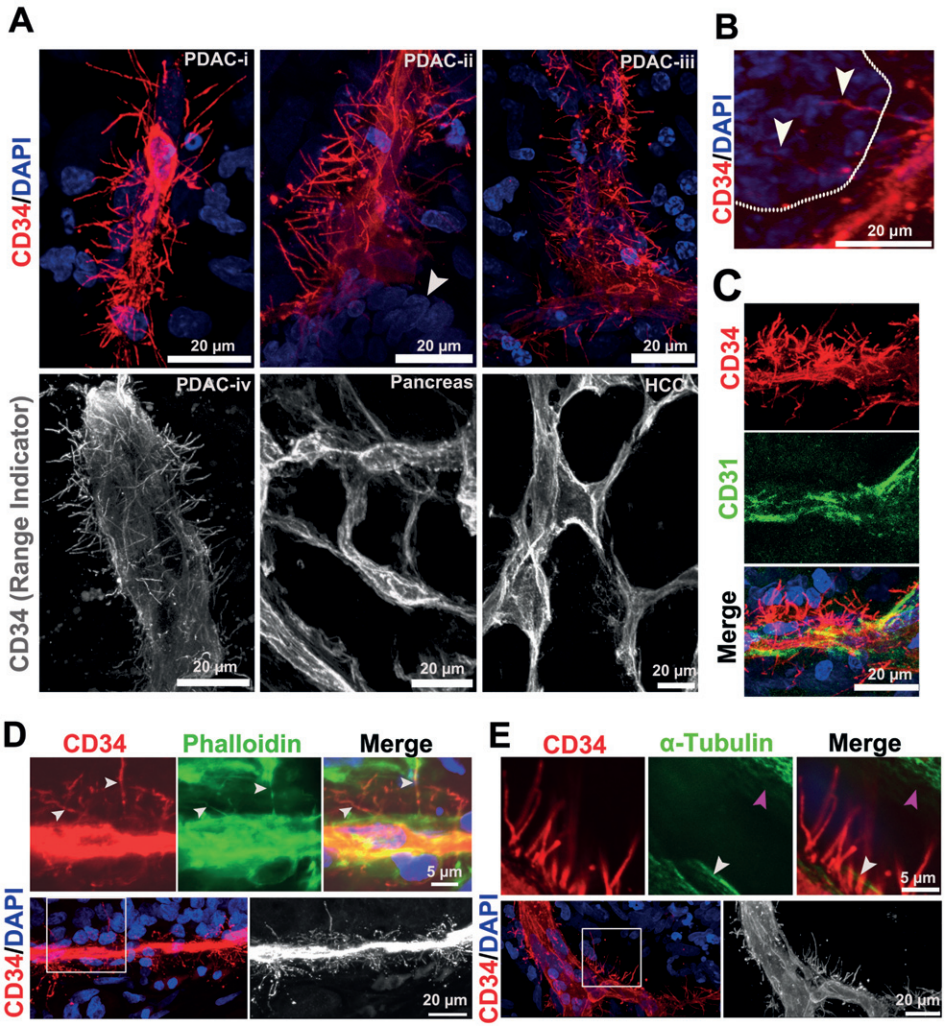


**Figure 2.** Basal microvilli are actin-rich vascular microprojections on the basal surface of PDAC microvessels. (A) CD34-immunostained 3D images of the basal surface appearance of PDAC, normal pancreas and HCC microvessels (PDAC microvessel diameters: i, 5 μm; ii, 10 μm; iii, 20 μm; iv, 35 μm); white arrow, neoplastic cells (see supplementary material, Movie S1). (B) Long basal endocilia invade into PDAC neoplastic cells (white dotted line represents the separation of neoplastic cell layer and stroma; white arrows, basal microvilli). (C) Co-immunostaining of basal microvilli with CD34 and CD31. (D) Co-immunostaining for phalloidin and CD34 labels the actin cytoskeleton of basal microvilli in PDAC tissue (white arrow, actin cytoskeleton and basal microvilli). (E) Co-immunostaining for α-tubulin and CD34 shows no α-tubulin in basal microvilli of PDAC endothelial cells; white arrow, endothelial cell; pink arrow, stroma cell.

[31–33]. Pancreatic neuroendocrine tumours (PanNETs) and haemangioblastomas (HBs) are highly angiogenic tumours, dependent upon activated VEGFR2 signalling [34–36]. However, little is known about the responsiveness of the PDAC vasculature to VEGFR2 signalling. Using co-immunostaining for VEGFR2 and its active form, phosphorylated VEGFR2$^{Y1175}$ (pVEGFR2$^{pY1175}$) and VEGFR2$^{Y996}$ (pVEGFR2$^{pY996}$) with CD34 in PDAC ($n = 8$), PanNET samples ($n = 3$) and HB ($n = 6$) tumour samples (see supplementary material, Table S3), PDAC microvessels had overall lower VEGFR2 expression (see supplementary material, Figure S2C), with a negative correlation between VEGFR2 and basal microvilli (Figure 4A). In contrast, PanNET and HB tumours showed high VEGFR2 expression along the entire microvessel membrane, including the filopodia (Figure 4A–C). Additionally, the microvasculature of PanNET and HBs had high pVEGFR2$^{Y1175}$ and pVEGFR2$^{Y996}$ expression, while the basal microvilli extending from the PDAC microvasculature had little to no pVEGFR2 reactivity (Figure 4C, D; see also supplementary material, Movie S3). These data suggest that, unlike microvessel growth seen in the angiogenic tumours, the microvessels and basal microvilli extending from the PDAC microvasculature have low levels of VEGFR2 expression and activation and, thus, may not depend on this signalling pathway for their growth and sustenance.

## Basal microvilli may enhance glucose trafficking between the microvessels and neoplastic cells

Based on the robust glucose uptake capacity seen in PDAC patients [7,37], we hypothesized that basal microvilli may serve as a conduit for glucose transport to neoplastic cells. $^{18}$FDG–PET is a functional imaging method that visualizes the glucose uptake ability of tumours *in vivo*, where the maximal standardized uptake

Copyright © 2015 Pathological Society of Great Britain and Ireland.
Published by John Wiley & Sons, Ltd. www.pathsoc.org.uk

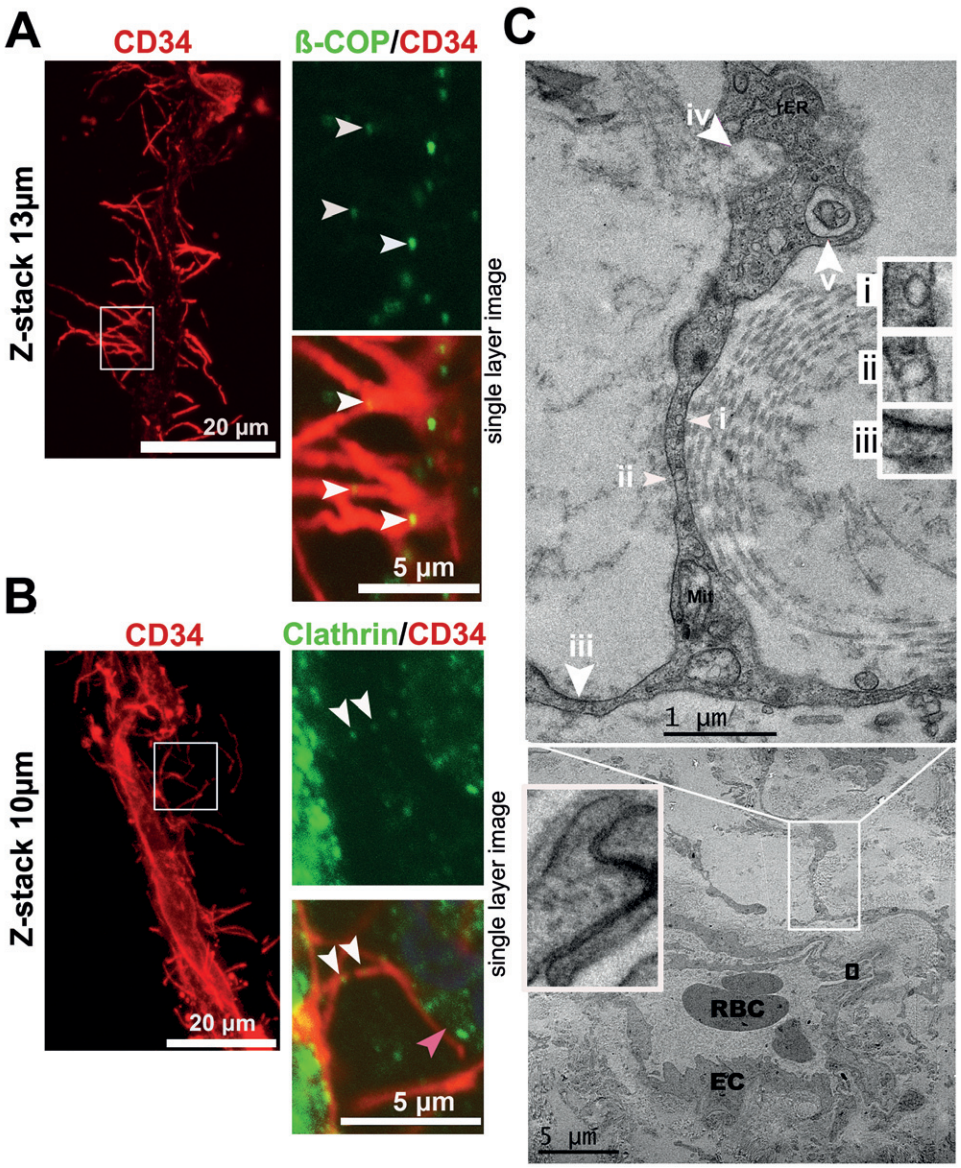


Figure 3. Basal microvilli have cellular uptake and trafficking capabilities. (A, B) Co-immunostaining for β-COP or clathrin with endothelial CD34 shows vesicular trafficking in basal microvilli in PDAC (white arrows, β-COP or clathrin-positive vesicles in microvilli; right panel, a single plane image). (C) Ultrastructural features of the basal microvilli of a microvessel in PDAC by TEM; i and ii, pinocytic vesicle; iii, macropinocytic pseudopodium with electron-dense particles on one side; iv, exocytosis; v, phagocytic vesicles; EC, endothelial cell; Mit, mitochondria; rER, rough endoplasm reticulum; RBC, red blood cells.

values ($SUV_{max}$) are used to semi-quantitatively estimate glucose uptake ability [38]. To determine whether there was a correlation of glucose concentration in the tumours relative to the presence of basal microvilli, we compared the characteristics of microvessels with basal microvilli in PDAC patients ($n = 7$) with different $SUV_{max}$ values. We quantified the lengths and densities of basal microvilli on microvessels in tumour regions and found that tumours with high glucose uptake had microvessels containing longer and denser basal microvilli, while tumours with lower glucose concentration had shorter and fewer basal microvilli on the tumour microvessel surface (Figure 5A, B; see also supplementary material, Figure S6A). As the rate of solute exchange of a cell depends on the size of its surface area, we determined that basal microvilli increased the surface area of the microvasculature, using an algorithm (see supplementary material, Supplementary materials and methods), and this correlated with high $SUV_{max}$ values from human patients (Figure 5B). However, patient $SUV_{max}$ values were not dependent upon the percentage of microvessels in the tumour (see supplementary material, Figure S6B).

Glucose uptake or transport in endothelial cells is facilitated by the glucose transporters (GLUT) family of transmembrane proteins, some via endocytosis and exocytosis [39], and this often depends on the actin cytoskeleton to transport in or through cells [40,41]. We co-immunostained for CD34, GLUT-1 and phalloidin to determine whether actin-containing basal microvilli contain GLUT-1-positive vesicles. Indeed, we detected GLUT-1-positive vesicles within the basal

Copyright © 2015 Pathological Society of Great Britain and Ireland.
Published by John Wiley & Sons, Ltd. www.pathsoc.org.uk

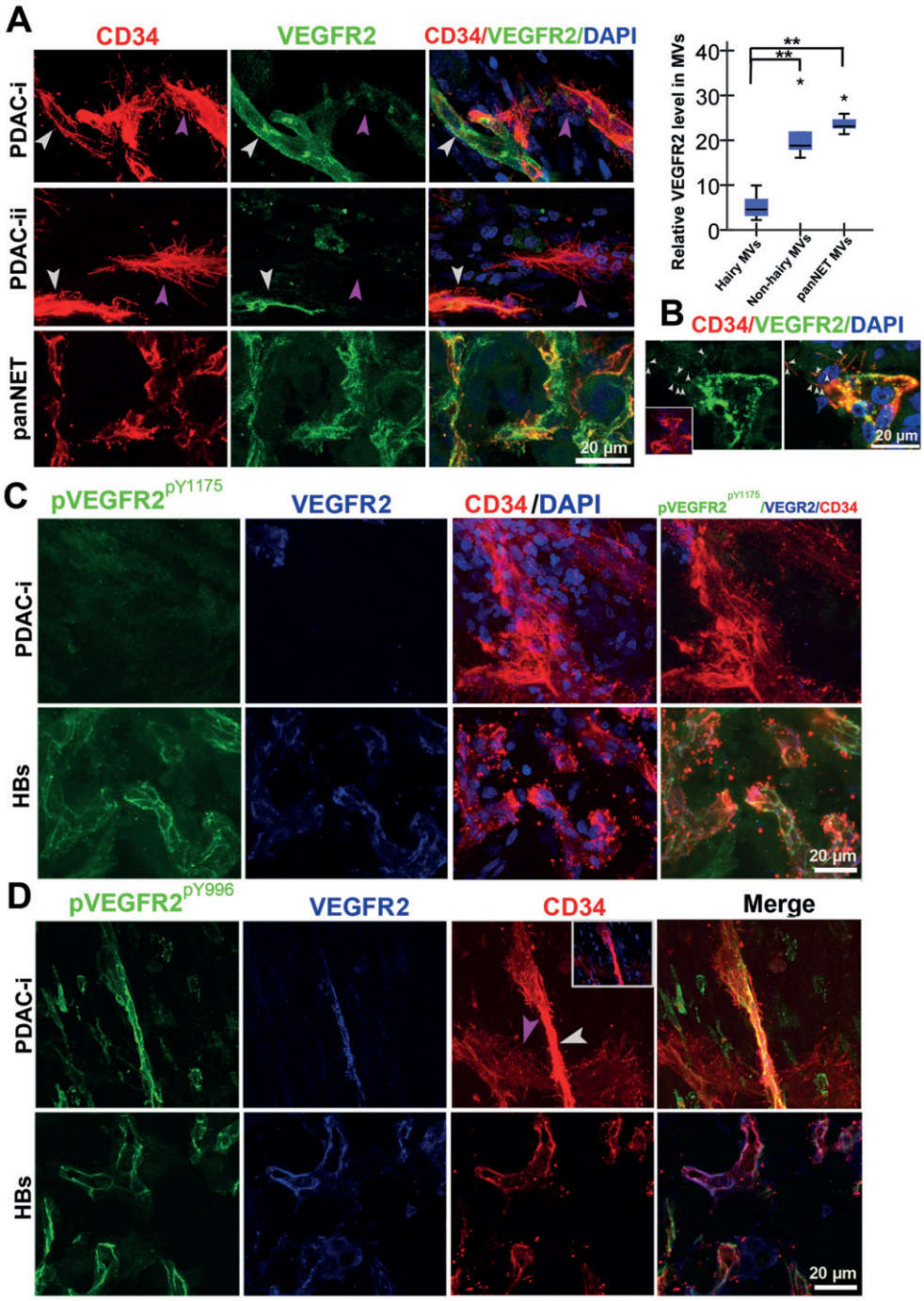


**Figure 4.** Low VEGFR2 expression and phosphorylation in microvessels that possess basal microvilli. (A) VEGFR2 expression patterns in PDAC 'hairy' or 'non-hairy'microvessels and PanNET microvessels and endothelial tip cells (PDAC, yellow arrows, 'non-hairy' microvessel; pink arrow, hairy microvessels; PanNET; small white arrows, VEGFR2-positive dots on filopodia). Quantitative analysis comparing VEGFR2 levels in 'hairy' microvessels with 'non-hairy'microvessels of PDAC and microvessels of PanNET. Statistical significance was assessed by Student's *t*-test. (B) VERGR2 expression patterns in terminal endothelial cells of the PanNET microvasculature (white arrows, VEGFR2-positive dots on filopodia). (C) Phospho-VEGFR2$^{Y1175}$ (pVEGFR2$^{Y1175}$) levels in 'hairy' microvessels of PDAC and microvasculature in HBs. (D) Phospho-VEGFR2$^{Y996}$ (pVEGFR2$^{Y996}$) levels in 'hairy' or 'non-hairy' microvessels of PDAC and microvasculature in HBs; white arrow, 'non-hairy' microvessels; pink arrow, 'hairy' microvessels (see supplementary material, Movie S3).

microvilli of microvessels that have active blood flow, and these GLUT1-positive vesicles co-localized with phalloin-positive actin filaments (Figure 5C, D; see also supplementary material, Movie S4). These data indicated that basal microvilli may have the ability to transport glucose into and out of the tumour milieu. While glucose concentration is difficult to assess directly in human tissues, it is well known that GLUT-1 levels are sensitive to changes in glucose concentration [42]. To address this possibility *in vitro*, we tested the sensitivity of MiaPaCa-2 cells to varying glucose concentrations. GLUT-1 expression was low in high-glucose medium, but high when glucose was absent from the medium (see

Copyright © 2015 Pathological Society of Great Britain and Ireland.
Published by John Wiley & Sons, Ltd. www.pathsoc.org.uk

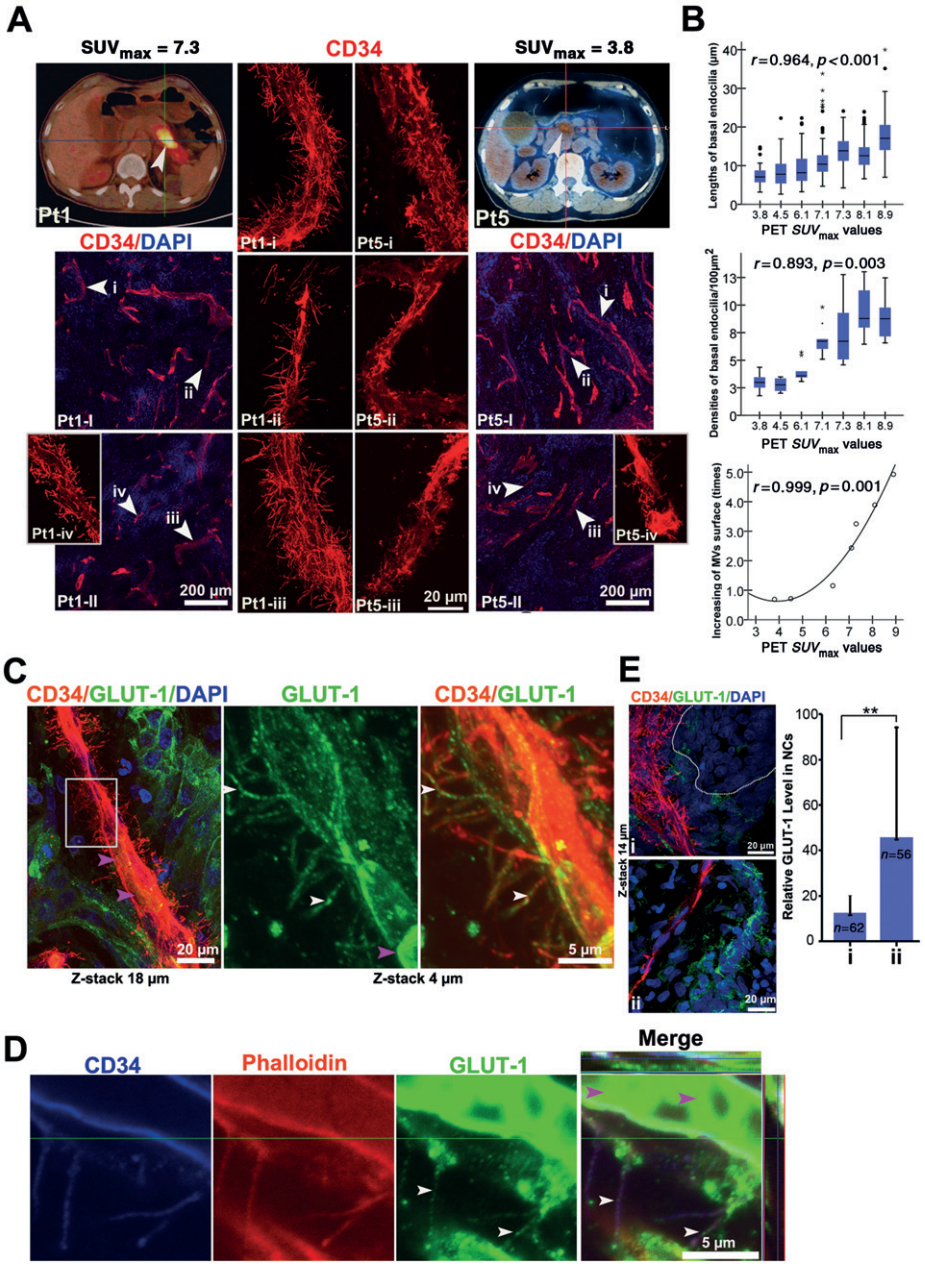


**Figure 5.** High glucose uptake in PDAC tumours with extensive basal microvilli. (A) Representative images of glucose uptake, using $^{18}$FDG–PET imaging and characteristics of basal microvilli in PDAC patients: $^{18}$FDG–PET images and 3D microvessel images of two PDAC patients (Pt1, a 68 year-old man with $SUV_{max} = 7.3$, tumour size = 5.20 × 2.60 cm: Pt5, a 74 year-old man with $SUV_{max} = 3.8$, tumour size = 2.52 × 1.92 cm); trans-axial PET images reveal high focal $^{18}$FDG accumulation in the region of the pancreatic body (Pt1) and moderate in head (Pt5); white arrows, tumour mass; scanning 60 min after injection of $^{18}$FDG. (B) Relationship between $SUV_{max}$ values of patients with the lengths and density of microvessel basal microvilli of seven patient tumours; statistical significances were performed by Spearman's correlation. (C) GLUT-1-positive basal microvilli on the PDAC microvasculature with RBCs in microvessel lumen: white arrows, GLUT-1-positive vesicles; pink arrow, RBCs (see supplementary material, Movie S4). (D) Co-immunostaining for phalloidin, CD34 and GLUT-1 showed that GLUT-1 vesicles co-localized with the actin cytoskeleton of basal microvilli on PDAC microvessels; white arrow, GLUT-1 vesicles; pink arrow, RBCs (see supplementary material, Movie S4). (E) GLUT-1 expression in areas of PDAC tumour with a high and low density of basal microvilli; circled regions, neoplastic ducts; *n*, neoplastic cell count.

supplementary material, Figure S6C). The change in GLUT-1 expression in MiaPaca-2 cells was seen within a few hours after glucose starvation (see supplementary material, Figure S6C). These data suggest that glucose concentrations have a significant effect on GLUT-1 expression in MiaPaCa-2 cells *in vitro*; thus, it is possible that GLUT-1 levels in neoplastic cells reflect the same glucose sensitivity *in vivo*. Although GLUT-1 expression in PDAC neoplastic cells is high, the distribution of GLUT-1 expression in neoplasia is spatial and appears in a gradient pattern, with some areas very high and some areas very low (see supplementary material, Figure S6D). Given the uneven GLUT-1 distribution in the tumour, we hypothesized that the presence of basal microvilli was dependent upon GLUT-1 expression and, therefore, co-immunostained

Copyright © 2015 Pathological Society of Great Britain and Ireland.
Published by John Wiley & Sons, Ltd. www.pathsoc.org.uk

PDAC tumours with GLUT-1 and CD34. Neoplastic cells with low GLUT-1 expression were in close proximity to microvessels with many long basal microvilli extending into the neoplastic cells, while those with high levels of GLUT-1 were not (Figure 5E; see also supplementary material, Figure S6E, F, Movie S5), implying that basal microvilli are inversely dependent upon GLUT-1 expression in neoplasia. Together, these data suggest that these vascular microprojections may play a role in helping the tumour meet its high glucose needs.

### KPC mouse tumours recapitulate pathological microvessels in human PDAC

To determine whether these basal microvilli could be studied in a genetically engineered mouse model (GEMM) for PDAC, we acquired tumour tissues from the well-established *LSL–Kras*$^{G12D/+}$; *LSL–Trp53*$^{R172H/+}$; *Pdx1–Cre* mouse model (hereafter called KPC), which recapitulates human PDAC pathology [43]. Thick tumour sections from KPC mice were co-immunostained with the aforementioned molecular and cellular markers to measure microvessel characteristics. Basal microvilli are also present on the basal surface of the tumour vasculature in KPC mice, but not in the near-normal regions within the same KPC sample, suggesting that these microvessels are pathological in this model (Figure 6A–C; see also supplementary material, Movie S6). Much like the human PDAC tumours, basal microvilli were widely distributed and contained actin microfilaments (Figure 6A, B). The length of basal microvilli in KPC tumours was similar to that seen in the human tumours, measuring about 5–41 μm. To determine whether the microvessels containing basal microvilli had a blood flow and whether the basal microvilli themselves had a functional lumen, we injected AlexaFluor 633-labelled lectin into the jugular veins of the KPC mice. As expected due to previous reports [19], we observed little to no fluorescent lectin within the microvessels themselves, making it impossible to determine whether the basal microvilli have a functional lumen (Figure 6C). Altogether, these findings suggest that the KPC mouse model recapitulates human PDAC vasculature, a novel discovery that will allow functional studies of the basal microvilli to be performed.

## Discussion

Using a modified immunostaining method, we discovered that PDAC tumours contain pathological vascular microprojections, or basal microvilli. Their actin-rich cytoskeleton and endo- and exocytic properties, along with their expression of GLUT-1 vesicles, suggest that their role is to increase the cell surface area of nutrient exchange of the tumour microvasculature. The presence and abundance of basal microvilli correlates positively with the high glucose uptake of human PDAC tumours. These data reveal an infinitesimal extension of the PDAC microvasculature that could support the metabolic demands of the growing tumour independent of conventional angiogenesis.

Endothelial cells in normal tissues have apical primary cilia that function as mechanical sensors [44–46] and filopodia that are present only in depolarized endothelial tip cells [47]. Filopodia on tip cells sense guidance cues in the microenvironment and facilitate endothelial cell migration, but do not have active endocytic or exocytic properties [48,49]. The evidence we present demonstrates a vascular structure that is unique and not a conventional endothelial filopodium, given the location of basal microvilli on the microvessel (on the basal, not the apical, surface), their distribution (extending from the stalk microvessel, not from a budding terminal endothelial cell) and their actin positivity (although it is possible that these unique vascular structures behave like filopodia through their actin-rich characteristics, this does not make them filopodia). In addition, basal microvilli contain both clathrin-dependent and clathrin-independent vesicles, implicating their role in both endo- and exocytosis, unlike filopodia. Phagocytic and macropinocytic properties are essential for clearing cell debris or macromolecules and tissue fluids to establish and maintain the composition of the tumour microenvironment [50]. Basal microvilli have pinocytic characteristics much like those of normal microvessels [51], possibly enhancing the phagocytic and macropinocytic activities of PDAC microvessels.

Oncogenic KRas$^{G12D}$, which is present in >90% of PDAC patients, shifts the metabolism of tumour cells from aerobic respiration to anaerobic glycolysis [52,53]. GLUT-1 is an important membrane transporter of glucose in endothelial cells and in *Ras*-mutated neoplastic cells [54,55]. Basal microvilli contain GLUT-1-positive vesicles and their abundance positively correlates with glucose uptake of human PDAC tumours, suggesting that the basal microvilli are responsible for trafficking glucose into the tumour cells. Furthermore, the spatial decrease in GLUT-1 expression in neoplastic regions of the tumour correlated with longer, denser basal microvilli on the tumour microvessels. Together, these factors suggest that the presence of basal microvilli is the microvasculature's response to meet the high metabolic demands of the tumour.

High glucose uptake or high blood glucose worsens the outcome of PDAC patients [56,57]. Although glucose may extravasate through intercellular junctions and/or pass through leaky vessels at the tumour periphery and diffuse through the tumour matrix, PDAC is mostly hypovascularized and contains a dense extracellular matrix, which impacts the biophysical and biochemical constraints on the microvasculature [58,59]. PDAC is also characterized by non-leaky microvessels with intact cellular junctions [60], suggesting that basal microvilli may have a significant role in the high uptake of glucose in PDAC. Importantly, basal microvilli are pathological and are not present

Copyright © 2015 Pathological Society of Great Britain and Ireland.
Published by John Wiley & Sons, Ltd. www.pathsoc.org.uk

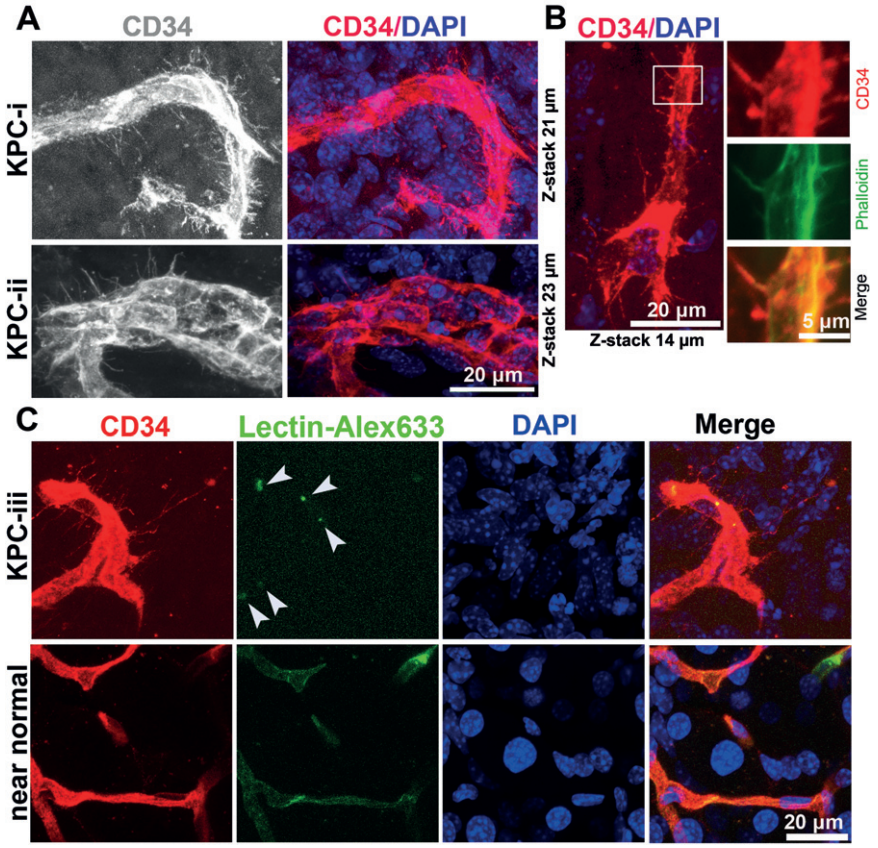


**Figure 6.** KPC mouse tumours recapitulate pathological microvessels of human PDAC. (A) 3D images of CD34-stained microvessels in KPC mouse tumours; microvessels diameter, 10 μm; microvessel diameter, 20 μm (see supplementary material, Movie S6). (B) Phalloidin and CD34 co-immunostaining reveals the actin cytoskeleton of basal microvilli in KPC tumour tissue; microvessels diameter, 5 μm. (C) 3D images of CD34-stained microvessels in KPC mouse tumours and near-normal KPC mouse tissue perfused by AlexaFluor 633-conjugated lectin; white arrow, lectin (see supplementary material, Movie S6).

in the microvasculature of normal tissues. This selective expression can be exploited in several therapeutic approaches. First, there is an opportunity to specifically and selectively target the tumour microvasculature, while sparing the normal vasculature using selective therapeutics against these vascular microstructures. Alternatively, it may be possible to target and ablate the glucose-trafficking basal microvilli as a method of starving the oncogenic $Kras^{G12D}$-dependent tumour cells. Targeting the glucose trafficking abilities of basal microvilli could cut off the lifeline of glucose to the tumour, causing it to regress and possibly improving a patient's outcome. Because the KPC mouse model recapitulates human basal microvilli, these hypotheses can be tested.

## Acknowledgements

This study was supported by the Ministry of Education Youth Teacher Fund (Grant No. KPH1322045), the Special Research Fund for Public Welfare Industry of Health and the Translational Research of Early Diagnosis and Comprehensive Treatment in Pancreatic Cancer from the Ministry of Health of China (Grant No. 201202007), the National Key Sci-Tech Special Project of China (Grant No. 2008ZX10002-020), the Project of the Shanghai Municipal Science and Technology Commission (Grant No. 03dz14086), the Changjiang Visiting Scholar Programme, and the American Cancer Society (Grant No. PF-13-317-01). The authors thank Professor Hongbin Lu and Mr Yulei Ren from Fudan University for help with TEM scanning, and Ms Frances Dressman for editorial assistance.

## Author contributions

HS discovered the basal microvilli in PDAC and designed the research project; HS, YWu, CMAA, YF, YWei and PZ performed experiments; YF, XH, JL and WL collected clinical samples; HS, CMAA, AM and DT analysed data; and SH, CMAA, QY, JL, DT and LY wrote the paper.

## References

1. Jemal A, Siegel R, Ward E, *et al.* Cancer statistics, 2009. *CA Cancer J Clin* 2009; **59:** 225–249.
2. Chu GC, Kimmelman AC, Hezel AF, *et al.* Stromal biology of pancreatic cancer. *J Cell Biochem* 2007; **101:** 887–907.

Copyright © 2015 Pathological Society of Great Britain and Ireland.
Published by John Wiley & Sons, Ltd. www.pathsoc.org.uk

3. Neesse A, Michl P, Frese KK, *et al.* Stromal biology and therapy in pancreatic cancer. *Gut* 2011; **60:** 861–868.
4. Stathis A, Moore MJ. Advanced pancreatic carcinoma**:** current treatment and future challenges. *Nat Rev Clin Oncol* 2010; **7:** 163–172.
5. Feig C, Gopinathan A, Neesse A, *et al.* The pancreas cancer microenvironment. *Clin Cancer Res* 2012; **18:** 4266–4276.
6. Provenzano PP, Hingorani SR. Hyaluronan, fluid pressure, and stromal resistance in pancreas cancer. *Br J Cancer* 2013; **108:** 1–8.
7. Serrano OK, Chaudhry MA, Leach SD. The role of PET scanning in pancreatic cancer. *Adv Surg* 2010; **44:** 313–325.
8. Karreth FA, Tuveson DA. Modelling oncogenic Ras/Raf signalling in the mouse. *Curr Opin Genet Dev* 2009; **19:** 4–11.
9. McDonald DM, Choyke PL. Imaging of angiogenesis: from microscope to clinic. *Nat Med* 2003; **9:** 713–725.
10. Yuan SY, Rigor RR. *In Regulation of Endothelial Barrier Function.* Morgan & Claypool Life Sciences: San Rafael, CA, 2010.
11. Hlatky L, Hahnfeldt P, Folkman J. Clinical application of antiangiogenic therapy: microvessel density, what it does and doesn't tell us. *J Natl Cancer Inst* 2002; **94:** 883–893.
12. Wang J, Dore S. Heme oxygenase-1 exacerbates early brain injury after intracerebral haemorrhage. *Brain* 2007; **130:** 1643–1652.
13. Schneider CA, Rasband WS, Eliceiri KW: NIH Image to ImageJ: 25 years of image analysis. *Nat Methods* 2012; **9:** 671–675.
14. Semela D, Dufour JF. Angiogenesis and hepatocellular carcinoma. *J Hepatol* 2004; **41:** 864–880.
15. van der Zee JA, van Eijck CH, Hop WC, *et al.* Angiogenesis: a prognostic determinant in pancreatic cancer? *Eur J Cancer* 2011; **47:** 2576–2584.
16. Carmeliet P, Jain RK. Angiogenesis in cancer and other diseases. *Nature* 2000; **407:** 249–257.
17. Jain RK, di Tomaso E, Duda DG, *et al.* Angiogenesis in brain tumours. *Nat Rev Neurosci* 2007; **8:** 610–622.
18. Olive KP, Jacobetz MA, Davidson CJ, *et al.* Inhibition of Hedgehog signaling enhances delivery of chemotherapy in a mouse model of pancreatic cancer. *Science* 2009; **324:** 1457–1461.
19. Jacobetz MA, Chan DS, Neesse A, *et al.* Hyaluronan impairs vascular function and drug delivery in a mouse model of pancreatic cancer. *Gut* 2013; **62:** 112–120.
20. Sun HC, Qiu ZJ, Liu J, *et al.* Expression of hypoxia-inducible factor-1α and associated proteins in pancreatic ductal adenocarcinoma and their impact on prognosis. *Int J Oncol* 2007; **30:** 1359–1367.
21. Dai CX, Gao Q, Qiu SJ, *et al.* Hypoxia-inducible factor-1α, in association with inflammation, angiogenesis and MYC, is a critical prognostic factor in patients with HCC after surgery. *BMC Cancer* 2009; **9:** 418.
22. Koong AC, Mehta VK, Le QT, *et al.* Pancreatic tumors show high levels of hypoxia. *Int J Radiat Oncol Biol Phys* 2000; **48:** 919–922.
23. Phng LK, Gerhardt H. Angiogenesis**:** a team effort coordinated by notch. *Dev Cell* 2009; **16:** 196–208.
24. Potente M, Gerhardt H, Carmeliet P. Basic and therapeutic aspects of angiogenesis. *Cell* 2011; **146:** 873–887.
25. Lu X, Le Noble F, Yuan L, *et al.* The netrin receptor UNC5B mediates guidance events controlling morphogenesis of the vascular system. *Nature* 2004; **432:** 179–186.
26. Vracko R, Benditt EP. Capillary lamina thickening. Its relationship to endothelial cell death and replacement. *J Cell Biol* 1970; **47:** 281–285.
27. Montel-Hagen A, Blanc L, Boyer-Clavel M, *et al.* The Glut1 and Glut4 glucose transporters are differentially expressed during perinatal and postnatal erythropoiesis. *Blood* 2008; **112:** 4729–4738.
28. Satir P, Christensen ST. Overview of structure and function of mammalian cilia. *Annu Rev Physiol* 2007; **69:** 377–400.
29. Lange K. Fundamental role of microvilli in the main functions of differentiated cells: outline of an universal regulating and signaling system at the cell periphery. *J Cell Physiol* 2011; **226:** 896–927.
30. Grant BD, Donaldson JG. Pathways and mechanisms of endocytic recycling. *Nat Rev Mol Cell Biol* 2009; **10:** 597–608.
31. Sinha S, Vohra PK, Bhattacharya R, *et al.* Dopamine regulates phosphorylation of VEGF receptor 2 by engaging Src-homology-2-domain-containing protein tyrosine phosphatase 2. *J Cell Sci* 2009; **122:** 3385–3392.
32. Cross MJ, Claesson-Welsh L. FGF and VEGF function in angiogenesis: signalling pathways, biological responses and therapeutic inhibition. *Trends Pharmacol Sci* 2001; **22:** 201–207.
33. Wedam SB, Low JA, Yang SX, *et al.* Antiangiogenic and antitumor effects of bevacizumab in patients with inflammatory and locally advanced breast cancer. *J Clin Oncol* 2006; **24:** 769–777.
34. Couvelard A, O'Toole D, Turley H, *et al.* Microvascular density and hypoxia-inducible factor pathway in pancreatic endocrine tumours: negative correlation of microvascular density and VEGF expression with tumour progression. *Br J Cancer* 2005; **92:** 94–101.
35. Raymond E, Dahan L, Raoul JL, *et al.* Sunitinib malate for the treatment of pancreatic neuroendocrine tumors. *N Engl J Med* 2011; **364:** 501–513.
36. Hatva E, Bohling T, Jaaskelainen J, *et al.* Vascular growth factors and receptors in capillary hemangioblastomas and hemangiopericytomas. *Am J Pathol* 1996; **148:** 763–775.
37. Higashi T, Saga T, Nakamoto Y, *et al.* Relationship between retention index in dual-phase $^{18}$F-FDG PET, and hexokinase-II and glucose transporter-1 expression in pancreatic cancer. *J Nucl Med* 2002; **43:** 173–180.
38. Friess H, Langhans J, Ebert M, *et al.* Diagnosis of pancreatic cancer by 2 $^{18}$F-fluoro-2-deoxy-D-glucose positron emission tomography. *Gut* 1995; **36:** 771–777.
39. Mueckler M. Facilitative glucose transporters. *Eur J Biochem* 1994; **219:** 713–725.
40. Klip A, Sun Y, Chiu TT, Foley KP. Signal transduction meets vesicle traffic: the software and hardware of GLUT4 translocation. *Am J Physiol Cell Physiol* 2014; **306:** C879–886.
41. Tsakiridis T, Vranic M, Klip A. Disassembly of the actin network inhibits insulin-dependent stimulation of glucose transport and prevents recruitment of glucose transporters to the plasma membrane. *J Biol Chem* 1994; **269:** 29934–29942.
42. Ogura K, Sakata M, Yamaguchi M, *et al.* High concentration of glucose decreases glucose transporter-1 expression in mouse placenta *in vitro* and *in vivo*. *J Endocrinol* 1999; **160:** 443–452.
43. Hingorani SR, Wang L, Multani AS, *et al.* Trp53R172H and KrasG12D cooperate to promote chromosomal instability and widely metastatic pancreatic ductal adenocarcinoma in mice. *Cancer Cell* 2005; **7:** 469–483.
44. Egorova AD, van der Heiden K, Poelmann RE, *et al.* Primary cilia as biomechanical sensors in regulating endothelial function. *Differentiation* 2012; **83:** S56–61.
45. Goetz JG, Steed E, Ferreira RR, *et al.* Endothelial cilia mediate low flow sensing during zebrafish vascular development. *Cell Rep* 2014; **6:** 799–808.
46. Jones TJ, Adapala RK, Geldenhuys WJ, *et al.* Primary cilia regulate the directional migration and barrier integrity of endothelial cells through the modulation of Hsp27 dependent actin cytoskeletal organization. *J Cell Physiol* 2012; **227:** 70–76.
47. Carmeliet P, Jain RK. Molecular mechanisms and clinical applications of angiogenesis. *Nature* 2011; **473:** 298–307.
48. Virgintino D, Rizzi M, Errede M, *et al.* Plasma membrane-derived microvesicles released from tip endothelial cells during vascular sprouting. *Angiogenesis* 2012; **15:** 761–769.
49. Niles WD, Malik AB. Endocytosis and exocytosis events regulate vesicle traffic in endothelial cells. *J Membr Biol* 1999; **167:** 85–101.


Copyright © 2015 Pathological Society of Great Britain and Ireland.
Published by John Wiley & Sons, Ltd. www.pathsoc.org.uk

50. Swanson JA. Shaping cups into phagosomes and macropinosomes. *Nat Rev Mol Cell Biol* 2008; **9:** 639–649.
51. Marchesi VT. The role of pinocytic vesicles in the transport of materials across the walls of small blood vessels. *Invest Ophthalmol* 1965; **4:** 1111–1121.
52. Biankin AV, Waddell N, Kassahn KS, *et al.* Pancreatic cancer genomes reveal aberrations in axon guidance pathway genes. *Nature* 2012; **491:** 399–405.
53. Ying H, Kimmelman AC, Lyssiotis CA, *et al.* Oncogenic Kras maintains pancreatic tumors through regulation of anabolic glucose metabolism. *Cell* 2012; **149:** 656–670.
54. Mann GE, Yudilevich DL, Sobrevia L. Regulation of amino acid and glucose transporters in endothelial and smooth muscle cells. *Physiol Rev* 2003; **83:** 183–252.
55. Calvo MB, Figueroa A, Pulido EG, *et al.* Potential role of sugar transporters in cancer and their relationship with anticancer therapy. *Int J Endocrinol* 2010; 2010.
56. Schellenberg D, Quon A, Minn AY, *et al.* $^{18}$Fluorodeoxyglucose PET is prognostic of progression-free and overall survival in locally advanced pancreas cancer treated with stereotactic radiotherapy. *Int J Radiat Oncol Biol Phys* 2010; **77:** 1420–1425.
57. Gapstur SM, Gann PH, Lowe W, *et al.* Abnormal glucose metabolism and pancreatic cancer mortality. *J Am Med Assoc* 2000; **283:** 2552–2558.
58. Neesse A, Michl P, Frese KK, *et al.* Stromal biology and therapy in pancreatic cancer. *Gut* 2011; **60:** 861–868.
59. Schima W, Fugger R, Schober E, *et al.* Diagnosis and staging of pancreatic cancer: comparison of mangafodipir trisodium-enhanced MR imaging and contrast-enhanced helical hydro-CT. *Am J Roentgenol* 2002; **179:** 717–724.
60. Jacobetz MA, Chan DS, Neesse A, *et al.* Hyaluronan impairs vascular function and drug delivery in a mouse model of pancreatic cancer. *Gut* 2013; **62:** 112–120.
61. *Toner PG, Carr KE, Ferguson A, *et al.* Scanning and transmission electron microscopic studies of human intestinal mucosa. *Gut* 1970; **11:** 471–481.

*Cited in supplementary material only.

## SUPPLEMENTARY MATERIAL ON THE INTERNET

The following supplementary material may be found in the online version of this article:

Supplementary materials and methods

**Figure SM1.** Steps to measure microvessel parameters.

**Figure SM2.** Calibrating the length of basal microvilli.

**Figure S1.** Correlation analysis of microvessel parameters and PDAC patient prognosis.

**Figure S2.** Low HIF-1α levels present in PDAC and high HIF-1a levels present in HCC.

**Figure S3.** PDAC microvessels are mature with high pericyte coverage, while HCC microvessels are immature with nascent and minimal pericyte coverage.

**Figure S4.** PDAC microvessels have a complete basement membrane.

**Figure S5.** Basal microvilli are present in the functional microvessels of advanced stage PDAC tumours.

**Figure S6.** Basal microvilli in PDAC may enhance glucose transport.

**Table S1.** Correlation of microvascular parameters and clinical pathological characteristics in patients

**Table S2.** Summary of pericyte characteristics

**Table S3.** Basic clinical characteristics of panNET and HBs patients

**Table S4.** List of antibodies and dyes

**Movie S1.** 3D demonstration of microvasculature with basal microvilli in PDAC tumours (PDAC i–iv) and 3D demonstration of normal pancreas and HCC tumour microvessels

**Movie S2.** 3D demonstration of Figure S4E and F.

**Movie S3.** 3D demonstration of Figure 4D.

**Movie S4.** 3D video of Figure 5C and D in *z* axis.

**Movie S5.**a 3D demonstration of spatial GLUT-1 expression in PDAC neoplastic cells in close proximity to long basal microvilli.

**Movie S6.** 3D demonstration of 'hairy' microvessels in KPC mouse tumour and microvessels in KPC mouse near normal pancreatic tissue.

Copyright © 2015 Pathological Society of Great Britain and Ireland.
Published by John Wiley & Sons, Ltd. www.pathsoc.org.uk